The validity of plagioclase-melt geothermometry for degassing-driven magma crystallisation.

Humphreys, Madeleine C. S.[1], Edmonds, Marie[2] and Klöcking, Marthe S.[2]

[1] Department of Earth Sciences, Durham University, Science Labs, Durham, DH1 3LE, UK. Tel: +44 (0)191 334 2343. Email: madeleine.humphreys@durham.ac.uk

[2] Department of Earth Sciences, University of Cambridge, Downing Street, Cambridge, CB2 3EQ, UK

Abstract

Any quantitative interpretation of the formation conditions of igneous rocks requires methods for determining crystallisation temperature. Accurate application of such thermobarometers relies on the attainment of equilibrium in the system to be studied. This may be particularly difficult in silicic magmas, where diffusivities are low and crystallisation kinetics sluggish. Moreover, progressive degassing of volatile-rich magmas during ascent can result in continuous changes in effective undercooling, causing particular problems in achieving equilibrium between melt and crystals that grow in response to decompression. We consider these problems in the context of plagioclase-melt equilibria for magmas undergoing decompression and degassing-driven crystallisation, using two published thermometers. The two thermometers show similar trends with key parameters but absolute temperatures can vary significantly. Analysis of decompression experiments conducted at constant temperature shows systematic variations in calculated temperature and equilibrium constant with varying decompression rate and quench pressure. This

indicates that an unrecognised lack of equilibration could result in significant temperature overestimates and potentially spurious results. This highlights the need to assess for equilibrium, and we discuss problems associated with some commonly used indicators of equilibration. Finally, retrospective analysis of published plagioclase-hosted melt inclusion suites from five subduction zone volcanoes shows systematic increases in calculated temperature and decreases in equilibrium constant with decreasing H_2O concentration. While this could represent the signature of latent heat of crystallisation, we suggest that such patterns should be treated with caution unless there is clear evidence of sustained equilibrium between plagioclase and melt during decompression.

Introduction

Thermometry and thermobarometry underpin igneous petrology as a quantitative science. An ability to place quantitative estimates of temperature and pressure on mineral ± melt assemblages observed in igneous rocks is fundamental to understanding the conditions of magma storage, fractionation, ascent and eruption, as well as melt generation processes, in any tectonic setting. For example, clinopyroxene-melt thermobarometry was used to demonstrate that individual eruptions in the Springerville volcanic field, Arizona, USA were derived from different source regions in a vertically extensive mush reservoir, with magma ponding levels influenced by changes in crustal rheology or density (Putirka and Condit 2003). Cashman and Blundy (2013) used knowledge of plagioclase-melt equilibria to reconstruct the pressure-temperature histories of individual,

48 complexly zoned plagioclase phenocrysts from Mount St Helens, USA. Hornblende
49 thermobarometry also appears to define vertically extensive crystallisation
50 conditions for magmas from Redoubt volcano (Alaska) and El Reventador
51 (Ecuador), amongst others (Ridolfi et al. 2010).

52 Although application of thermobarometry is now routine, it still has the
53 potential to prompt new interpretations about the ways that magmas evolve and
54 migrate. For example, Blundy et al. (2006) used the plagioclase-liquid thermometer
55 of Putirka (2005) to determine entrapment temperatures for suites of plagioclase-
56 hosted melt inclusions. The results showed strong increases in calculated
57 temperature with decreasing melt H_2O contents, interpreted as the result of latent
58 heat release during exothermic, decompression-driven crystallisation of volatile-
59 saturated silicic magmas. This is significant because such release of latent heat could
60 produce commonly observed petrographic features, such as reversely zoned
61 phenocryst rims, that might otherwise be ascribed to late-stage mingling with hotter
62 magma (Blundy et al. 2006). With the increasing availability of relatively large
63 mineral and/or melt datasets from electron microprobe and other analytical
64 techniques, thermometers are now routinely applied to whole datasets instead of
65 carefully chosen individual analyses. This has the potential to uncover subtle details
66 that are only apparent at the population level, but brings a risk of inadequate
67 interrogation of equilibration within the full dataset.

68 An important limitation is that in volcanic systems, where the timescales of
69 melt crystallisation, chemical diffusion or magma movement may be short,
70 geochemical equilibration between melt and mineral may be kinetically inhibited.

For example, both the major element composition and the trace element contents of crystals are highly dependent on the degree of undercooling below the liquidus temperature (e.g. Gamble and Taylor 1980; Kennedy et al. 1993; Dunbar et al. 1995; Mollo et al. 2010, 2011b). Chemical diffusion rates can also be strongly dependent on the concentrations of species that are involved in the reaction(s). This is not a new problem and has been addressed by several authors historically, but is particularly important in the context of degassing-driven processes in volatile-rich magmas. In the context of thermobarometry, these factors represent varying degrees of disequilibrium and have the potential to produce biased or spurious temperatures if this is not recognised (e.g. Putirka 2008; Mollo et al. 2011b). In particular, Mollo et al. (2010) and Mollo et al. (2011b) showed that increasing the cooling rate of anhydrous basaltic melt from 0.5 to 15 °C/min could generate an overestimate in calculated temperature of up to 150 °C.

Here, we highlight the problems of not recognising incomplete equilibration in H_2O-bearing magmas, many of which crystallise due to decompression rather than cooling (e.g. Geschwind and Rutherford 1995; Blundy and Cashman 2001), where diffusivities are low and crystallisation kinetics may be very sluggish. In this scenario, the *thermal* undercooling driving crystallisation may be negligible but substantial effective undercoolings are still readily achieved by decompression and water loss. We focus on plagioclase-melt thermometry and degassing-driven magma crystallisation, which is particularly sensitive to the kinetics of crystal nucleation and growth. Drawing on previously published natural datasets and experimental studies, we demonstrate that disequilibrium crystallisation during degassing can

result in large errors in thermometry, and that this can lead to potentially very significant problems with obtaining a unique interpretation of the resultant P-T conditions.

Plagioclase-melt thermobarometry

Plagioclase-melt thermometers are based on equilibrium exchange of albite (Ab) and anorthite (An) components between solid (s) and melt (m):

$$An_{(m)} + Ab_{(s)} = An_{(s)} + Ab_{(m)} \quad [1]$$

with the equilibrium constant for An-Ab exchange expressed as (Putirka 2005; Putirka 2008):

$$K_D = (X_{An}^{pl} * Ca^L * Al^L) / (X_{Ab}^{pl} * Na^L * Si^L) \quad [2]$$

where (e.g.) Ca^L refers to the anhydrous cation fraction of Ca in the liquid and X_{An} is the mole fraction of anorthite in plagioclase. The composition of plagioclase crystallising from a melt is controlled by temperature, melt composition and melt H_2O concentration. In anhydrous melts, the equilibrium plagioclase composition shifts systematically towards albite with decreasing temperature (e.g. (Bowen 1913; Kudo and Weill 1970; Drake 1976). In hydrous melts, the shape of the albite-anorthite binary loop in T-X space is broadened and shifted to lower temperature relative to anhydrous compositions (Kudo and Weill 1970; Drake 1976; Johannes 1984). This may be because OH tends to complex with Na and SiO_4 groups in preference to Ca and AlO_4, particularly at higher temperature (Lange et al. 2009). This means that addition of H_2O causes a decrease in activity of the albite component of the melt, aAb(m), relative to aAn(m) and the liquidus plagioclase

117 composition therefore becomes more calcic (e.g. Arculus and Wills 1980; Housh and
118 Luhr 1991; Sisson and Grove 1993; Panjasawatwong et al. 1995).
119
120 We focus on two of the most recently published plagioclase-melt thermometers:
121 model A of Putirka (2005) and the plagioclase-melt hygrometer of Lange et al.
122 (2009). The latter has been recalibrated and updated by Waters and Lange (in
123 press). Both models are based on empirical regression of thermodynamically
124 derived expressions. Calibration of both models was done using large databases of
125 phase equilibrium experiments that crystallised plagioclase over a range of
126 pressures, temperatures and H_2O concentrations. A second set of experiments was
127 used to test each model. The Putirka model (model A) was calibrated on basaltic to
128 rhyolitic liquids that crystallised plagioclase from 0.001-13 kbar, 998-1623 K and
129 H_2O concentrations up to 15 wt%. According to the test data, the model returns
130 temperature with a standard error estimate of ± 23 K (Putirka 2005). A later
131 independent test using a larger dataset of additional experiments gave an average
132 absolute deviation of ±19 °C and propagated uncertainty of ± 7 MPa for experiments
133 on hydrous rhyolite at 750-995 °C and 15-313 MPa (Blundy et al. 2006). The Lange
134 et al. (2009) hygrometer was calibrated on rhyolitic melts with <30 vol% crystals at
135 925-1100 °C, 48-300 MPa and 2.2-7.0 wt% H_2O. Temperatures were recovered for
136 the test data with an average uncertainty of ± 14 °C, while the standard error
137 estimate for H_2O was ± 0.32 wt% (Lange et al. 2009).
138
139 **Comparison of the thermobarometers**

We first used each of the two thermometers to predict the shape of constant-X_{An} contours in H_2O-T space (figure 1) for a representative rhyolitic matrix glass composition from Soufrière Hills volcano, Montserrat (table 1), for comparison with the experimental study of Couch et al. (2003). For the Lange thermometer, this involved supplying X_{An}, T, P and melt composition to the model and retrieving melt H_2O over a range of temperatures. We ran these calculations using pressures of 10 MPa and 200 MPa, but this made little difference to the absolute H_2O concentrations retrieved and had no effect on the shape of the X_{An} contours. We therefore subsequently assumed H_2O-saturated conditions and calculated $P_{tot} = pH_2O$ using VolatileCalc (Newman and Lowenstern 2002) (we define pH_2O as the partial pressure of H_2O, which for a pure H_2O magmatic component is the total confining pressure at volatile saturation for a given H_2O concentration). For the Putirka thermometer we supplied X_{An}, H_2O content, P and melt composition and retrieved temperature, again assuming that $P_{tot} = pH_2O$.

Both models calculate an increase in temperature with decreasing H_2O concentration at constant X_{An} and fixed melt composition (figure 1a), as expected. Equivalent calculations using a basaltic-andesite melt from Hamada & Fujii (2007; see table 1) produce parallel curves offset to higher temperature at the same H_2O concentration. However, the overall results are highly model-dependent, particularly at low H_2O concentrations where there are big disparities between temperatures predicted for a given X_{An}. For example, at 20 MPa (1.3 wt% H_2O, volatile-saturated) plagioclase of composition An_{70} is predicted to occur in H_2O-

saturated melt at 951 °C using Putirka (2005) but at >1300 °C using Lange et al. (2009) (figure 1a). This indicates that application of plagioclase-melt equilibria to give *absolute* temperature estimates must be subject to at least some uncertainty. Data from the phase equilibrium experiments of Couch et al. (2003), which were used as a calibration dataset for Lange et al. (2009) but not for Putirka (2005), lie between the two models (figure 1a).

Figure 1

Secondly, we calculated temperature contours in H_2O – X_{An} space, which show a positive correlation of X_{An} with H_2O concentration at constant temperature (figure 1b). The results are similarly model-dependent, with only minor variations in slope of the temperature contours but significant variations in the absolute H_2O concentration predicted to be in equilibrium with a given plagioclase composition. In comparison, RhyoliteMELTS (Gualda et al. 2012) isothermal decompression runs and the data from Couch et al. (2003) show a much steeper variation of X_{An} with H_2O (figure 1b).

Figure 2

Finally, we calculated isobaric contours for H_2O-saturated rhyolite in T-X_{An} space; these define a positive correlation of temperature with X_{An} (figure 2). The two models agree well at lower temperature and more sodic plagioclase compositions

but diverge with increasing temperature and X_{An}. RhyoliteMELTS isobaric cooling runs are offset towards lower temperature and lower X_{An}, and with steeper slope in T-X_{An} space, than either of the other two thermobarometers (figure 2). The data from Couch et al. (2003) are offset to higher X_{An} relative to the Lange model and have a steeper slope than the Putirka model (figure 2).

Figure 3

As a possible test for equilibrium in the system $Ca_2Al_2Si_2O_8$ – $NaAlSi_3O_8$ – H_2O – silicate melt, the equilibrium constant for Ab-An exchange, K_D (equation [2]) is reported to be normally distributed with values of 0.10 ± 0.05 for T < 1050 °C (mostly hydrous) and 0.27 ± 0.11 for T ≥ 1050 °C, for a global compilation of test data (Putirka 2008). To assess the significance of individual external parameters in contributing to this variation, we retrieved K_D from the equilibrium calculations described above, using the Putirka thermometer. Importantly, the results show that for a fixed melt composition and fixed H_2O concentration *at equilibrium conditions*, variations in X_{An} cause K_D to decrease systematically with increasing temperature (figure 3a). Similarly, for a fixed melt composition at equilibrium at a constant calculated temperature, the link between X_{An} and pH_2O means that K_D decreases systematically with increasing X_{An} or increasing pH_2O (figure 3b,c). These variations mean that the equilibrium constant cannot easily be used to assess whether equilibrium has been achieved.

pH_2O – T profiles of decompression experiments

Both thermobarometers were originally calibrated and tested using phase equilibrium studies at fixed P, T conditions. However, many of their potential applications are for magmas that have experienced more dynamic conditions, including degassing-induced crystallisation. To test the applicability of the thermobarometers for these conditions in natural volatile-rich magmas, we used the results of three sets of decompression experiments that crystallised plagioclase from hydrous, silicic melt at variable decompression rates representative of typical intermediate magma ascent. Cichy et al. (2011) performed isothermal decompression experiments on a synthetic, H_2O-bearing Unzen rhyodacite melt composition at 850 °C and at decompression rates from 0.0002 to 20 MPa/s. Glass H_2O contents were analysed by FTIR but represent incomplete (disequilibrium) degassing due to retarded bubble nucleation (Cichy et al. 2011). Secondly, Martel and Schmidt (2003) ran both isobaric and decompression experiments on H_2O-saturated, synthetic rhyolitic melt at 860 °C and 15-170 MPa, at decompression rates from 0.000017 – 16 MPa/s. Thirdly, Brugger and Hammer (2010) performed two series of experiments using used a crushed natural rhyodacitic starting material: one set of experiments was quenched along a decompression path ('snapshots') and the other set was allowed to anneal at the final pressure. Decompression rates varied between 0.008 and 0.17 MPa/s. For each experimental dataset, we took the glass composition, H_2O concentration of the glass (either calculated as volatiles by difference or from published measurements, see supplementary data table) and coexisting plagioclase composition to calculate the

equilibrium temperature (T_{calc}, see supplementary data table). Except for mixed volatile (H_2O+CO_2) experiments we assumed melt H_2O saturation, and used VolatileCalc (Newman and Lowenstern 2002) to convert H_2O concentration to pH_2O in MPa. This is important because in all three experimental studies, H_2O degassing was retarded relative to equilibrium, showing higher concentrations in the glass than the solubility at the experimental quench pressure (figure 4). Treating the data in this way as volatile-saturated 'unknowns' therefore results in anomalously high estimates of P_{tot}.

Figure 4

Application of the Putirka thermometer to data from the Martel and Schmidt (2003) and Brugger and Hammer (2010) experimental series shows a general pattern of increasing T_{calc} and decreasing K_D with decreasing pH_2O (figure 5), even though the experiments were run at controlled temperature. Temperatures calculated from the 'low pressure' experiments of Martel and Schmidt (2003) are scattered within ± 45 °C of the experimental run temperature (860 ± 5 °C, Martel and Schmidt 2003), whereas the 'high pressure' experiments are systematically offset to significantly higher calculated temperatures, up to 84 °C greater than the experimental run temperature (figure 5). Their isobaric experiments also show an increase of T_{calc} with lower H_2O measurements (see supplementary data table). In contrast, temperatures for data from the Brugger and Hammer (2010) experiments are typically lower than the experimental run temperature (figure 5). The glass

compositions in all experiments show clear trends of increasing K_2O and decreasing CaO content as pH_2O decreases due to progressive decompression, degassing and crystallisation (see supplementary data table). The annealed experiments from Brugger and Hammer (2010) had a more Al-poor, K-rich and Si-rich residual melt composition and crystallised more albitic plagioclase; consequently temperatures calculated from these data are slightly lower at a given pH_2O than the snapshot experiments.

Figure 5

Temperatures calculated from Martel and Schmidt (2003) generally show an increase with increasing decompression rate except at the very highest decompression rates (>10 MPa/s); calculated K_Ds increase systematically with increasing decompression rate (figure 6) and with T_{calc} (supplementary data table). In contrast, the Brugger & Hammer data show no variation of either T_{calc} or K_D with decompression rate (figure 6), and no variation of K_D with T_{calc}, over the more limited range of decompression rates (see supplementary data table).

Figure 6

Fewer data are available for the Cichy et al. (2011) experiments but the available data give higher (and more scattered) calculated temperatures and lower K_D at lower pH_2O (figure 5). In contrast, there are clear increases in both T_{calc} and K_D with

278 increasing decompression rate, similar to calculations from the experiments of
279 Martel & Schmidt (figure 6), and K_D increases systematically with T_{calc} (see
280 supplementary data table). The glass compositions also change systematically as a
281 function of both pH_2O and decompression rate (supplementary data table).
282
283 The same patterns of T_{calc} are also seen using the Lange et al. (2009)
284 thermometer. The two sets of calculated temperatures correlate reasonably well but
285 those calculated using Lange et al. (2009) are typically significantly higher.
286 Meaningful temperatures commonly cannot be returned for evolved melts with low
287 H_2O content. This is due to an instability in the calculation of aAb(m) for
288 temperatures ≥1200 °C, which has been corrected by the recalibrated version of the
289 hygrometer (Waters and Lange in press; Lange & Waters, personal communication).
290 For this reason, and because the same trends were observed with both models, we
291 only used the Putirka thermometer for subsequent analysis of natural datasets (see
292 below).
293

294 **pH_2O-T profiles of magmas recorded in melt inclusions**

295 We applied a similar approach to populations of plagioclase-hosted melt inclusions
296 where the composition of coexisting melt and feldspar and the H_2O content of the
297 melt are both known, following Blundy et al. (2006). This allowed us to calculate the
298 apparent equilibrium temperature of entrapment for each melt inclusion and
299 plagioclase host pair, resulting in arrays of pH_2O-T coordinates (see supplementary
300 data table) and thus apparent magma ascent paths in pH_2O-T space. We examined

suites of melt inclusion data from the literature for Mount St Helens, USA (Blundy et al. 2006); Shiveluch Volcano, Kamchatka (Blundy et al. 2006); Soufrière Hills, Montserrat (Humphreys et al. 2009a, 2010); Unzen, Japan (Botcharnikov et al. 2008) and Izu-Oshima, Japan (Hamada and Fujii 2007). All datasets show a clear increase in T_{calc} with decreasing melt H_2O (figure 7), approximately parallel to constant-X_{An} contours shown in figure 1, as previously reported for Mount St Helens and Shiveluch by Blundy et al. (2006). There is a slight positive correlation of T_{calc} with X_{An} for the dataset as a whole (figure 7). For the rhyolitic melts (Soufrière Hills, Mount St Helens and Shiveluch), calculated K_Ds are low and typically decrease systematically with increasing X_{An} in the host plagioclase and increase systematically with increasing melt H_2O concentration (figure 8); the latter is the opposite to the trend observed for the equilibrium calculations (see figure 3). Calculated K_Ds are higher for the andesitic (Unzen) and basaltic andesite (Izu Oshima) melts but the same trends are observed (figure 8).

Figure 8

Regression of T_{calc} for each dataset with the individual parameters that contribute to the temperature calculation typically gives $R^2 \leq 0.92$ for correlation of T_{calc} with H_2O and low to insignificant R^2 (typically ≤ 0.25) for other parameters (figures 9, 10). This indicates that up to 92% of the total variability in T_{calc} from each case study results from variability in melt H_2O concentrations, typically with little effect of changing melt or plagioclase composition. This is reinforced by the fact that

'ruptured' melt inclusions (those known from their major element composition to have leaked H_2O, Blundy and Cashman 2005; Blundy et al. 2008) give anomalously high calculated temperatures, some in excess of 1000 °C (figure 7; supplementary data table). In fact, the full range of T_{calc} recorded by each dataset can be reproduced by manually changing the H_2O concentration of any individual inclusion, whereas the host plagioclase composition has relatively little effect on T_{calc}.

Figures 9, 10

Discussion

Degassing-induced crystallisation under disequilibrium conditions?

Our analysis shows that many arc magmas (all those examined) show evidence of apparent heating during degassing-induced crystallisation driven by decompression. Decreasing melt H_2O concentration is the primary factor that drives the increase in calculated temperature, accounting for up to 92% of the observed variations in T_{calc}. Experimental studies where volatile-saturated melt is decompressed at constant temperature also show the same effect, giving systematic increases in T_{calc} with decreasing melt H_2O concentration. Studies that covered a wide range of decompression rates also show a systematic increase of T_{calc} with increasing decompression rate, although the Brugger & Hammer dataset shows that absolute temperature may not always be overestimated (see below). Finally, the equilibrium constant for reaction of plagioclase and melt also varies systematically with both melt H_2O concentration and decompression rate. These observations

suggest that the calculated temperatures in the systems examined may reflect a disequilibrium process of volatile degassing and melt crystallisation. This could arise because crystal and bubble nucleation and growth at low pH_2O is hindered by the increasing diffusivities of components within the melt, which are intimately linked to degassing kinetics and temperature (e.g. Cashman and Blundy 2000; Hammer and Rutherford 2002; Couch et al. 2003b; Brugger and Hammer 2010). A lack of equilibrium in the decompression experiments is evidenced by variations in crystal size distribution and degree of plagioclase saturation, and progressive changes towards disequilibrium crystal morphologies with increasing decompression rate (Brugger and Hammer 2010). The slow equilibration process is also indicated by the slightly lower calculated temperatures retrieved (see figure 5) and more Ab-rich plagioclase crystallised in their series of experiments that were annealed at constant temperature following decompression, and by the failure of the MELTS algorithm to predict melt compositions for experiments quenched at <45 MPa (Brugger and Hammer 2010). Finally, the systematic variations of K_D with temperature, pH_2O and decompression rate in the experimental studies clearly show that these do not represent equilibrium conditions.

All the experimental studies examined here report a range of plagioclase compositions for each run. Plagioclase compositions closest to equilibrium are typically found at the crystal rim, with early-formed, more calcic plagioclase preserved in the cores (Martel and Schmidt 2003; Brugger and Hammer 2010; Waters 2013). This is explained by crystallisation during increasing extents of

effective undercooling, ΔT_{eff} (defined as $T_{liquidus} - T_{magma}$, see Crabtree and Lange 2011). Initially, crystallisation is inhibited relative to the equilibrium case, resulting in lower volumes of plagioclase growth; insufficient time available for complete re-equilibration means that as melt H_2O continues to change, new growth is added as more Ab-rich plagioclase, closer to equilibrium compositions (Brugger and Hammer 2010).

How accurate are calculated temperatures?

There is poor agreement between the two thermometers examined here, except for H_2O-rich melts and more albitic plagioclase (see figures 1 and 2). This means that it is difficult to be confident about the significance of absolute calculated temperatures, although relative variations appear robust. Secondly, crystallisation temperatures can be significantly over-estimated in the system plagioclase-melt-H_2O if disequilibrium is not recognised. This is consistent with observations of (Mollo et al. 2010, 2011) for both plagioclase and clinopyroxene in anhydrous basalt. Such disequilibrium would most likely take the form of hindered H_2O degassing into vesicles, disequilibrium crystallisation of anomalously An-rich plagioclase, or (for melt inclusions) variable loss of H from the inclusions after entrapment (see later). Our analysis shows that increases in T_{calc} can reflect increasing ΔT_{eff} due to changes in melt H_2O during decompression, as the melt viscosity increases and the kinetics of crystallisation become sluggish, rather than real increases in magma temperature. This means that, without an independent measure of ΔT_{eff}, it is difficult to interpret significant increases in calculated

393 temperature during magma ascent as unequivocally due to latent heat of
394 crystallisation (Blundy et al. 2006).
395
396 Substantial release of latent heat is, however, predicted on theoretical grounds,
397 because the primary driving force for crystallisation during decompression of
398 volatile-saturated magma is H_2O loss from the melt (Blundy et al. 2006).
399 Thermodynamic calculations indicate that plagioclase crystallisation from an
400 anhydrous melt would result in temperature increase of ~2.3 °C per 1%
401 crystallisation (Couch et al. 2001), while the assemblage plagioclase +
402 orthopyroxene + oxides would give ~3.2 °C per 1% (Blundy et al. 2006). For the
403 natural datasets studied here, the temperatures estimated from plagioclase-liquid
404 thermometry are typically well matched by two-oxide temperatures, including for
405 Mount St Helens and Shiveluch (Blundy et al. 2006) and Soufrière Hills, Montserrat
406 (two-oxide microphenocryst or microlite temperatures 958-1017 °C, Humphreys et
407 al. 2009b; temperatures up to ~968 °C from plagioclase-liquid thermometry, this
408 study). For Unzen, oxide equilibria indicate that the pre-eruptive magma was stored
409 at ~790 °C whereas groundmass oxides give temperatures of ~890 °C (Venezky &
410 Rutherford 1999), and plagioclase-liquid temperatures are significantly higher
411 (900–1080 °C, see figure 10). However, we note that even though in some cases
412 plagioclase-liquid temperatures calculated from Putirka (2005) and 2-oxide
413 temperatures are very similar, the available two-oxide temperatures would not be
414 in agreement with any of the plagioclase-liquid temperatures calculated using the
415 Lange et al. (2009) model. Variably high 2-oxide temperatures may otherwise be

ascribed to magma mixing immediately prior to eruption (e.g. Devine et al. 2003; Blundy et al. 2006).

We are not aware of any further temperature estimates for Izu Oshima volcano, but Hamada and Fujii (2007) interpreted the variations in H_2O concentration in their melt inclusion suite as the result of variable H_2O loss from the inclusions. A similar interpretation has been proposed to explain the variable H_2O contents of plagioclase-hosted melt inclusions from Soufriere Hills Volcano, as a result of rapid diffusional re-equilibration of H_2O through the phenocryst host (Mann et al. 2013). If this were the case, then the significant increase in calculated temperature seen in both datasets would result from disequilibrium driven by diffusive H loss from the inclusions, with the inclusion and host unable to re-equilibrate except on much longer timescales. This is effectively equivalent to the 'ruptured' melt inclusions from Mount St Helens (Blundy et al. 2008), which are known to have undergone syneruptive leakage of H_2O and which give anomalously high calculated temperatures (see figure 7).

Although overall the data from the decompression experiments show similar patterns of calculated temperature, there are also clear differences between studies. The experiments of Martel and Schmidt (2003) and Cichy et al. (2011) give calculated temperatures that are mostly too high, and are consistent with experimental run conditions only at high pH_2O (figure 5c, e) and for the 'low pressure' series of Martel & Schmidt (2003). However, the Brugger and Hammer

(2010) dataset consistently underestimates the known experimental run conditions, even though the same pattern of increasing temperature with decreasing pH_2O is still observed (figure 5a). A potentially significant difference between these studies is that Brugger and Hammer (2010) used a crushed natural starting material while both Martel and Schmidt (2003) and Cichy et al. (2011) used synthetic starting materials made from mixed powders. The use of different starting materials could affect the degree of approach to equilibrium during the experiments, particularly for experiments that cover a broad range of P-T-H_2O conditions (Pichavant et al. 2007).

An important final question is how to assess the accuracy of calculated temperatures, or ΔT_{eff}, in natural magmas. For the experiments, accuracy is simple to gauge by comparison with the known experimental temperature. However, for natural melt inclusion datasets (or crystal rim – host melt pairs) this is impossible without an independent measure of temperature and/or ΔT_{eff}. Any calculated temperature using the plagioclase-liquid thermometer should therefore be considered as a maximum unless there is clear evidence of equilibrium (see below). Ideally, ΔT_{eff} should be constrained independently, but in practice this is difficult. Integration of quantitative or qualitative textural studies with minor or trace element partitioning, which is known to be strongly dependent on ΔT (e.g. Gamble and Taylor 1980), may represent one path towards obtaining a less equivocal measure of the degree of disequilibrium in natural systems. However, we suggest that calculated K_D that are within the 'equilibrium range' of 0.10 ± 0.05 (for

462 temperatures < 1050 °C, Putirka 2008) are not sufficient to indicate complete
463 equilibration. Even the isobaric experiments of Martel and Schmidt (2003) show a
464 small but systematic decrease in K_D from 0.06 to 0.03 for a pressure range of 170 to
465 50 MPa, and this also reflects our calculations at fixed pH_2O and melt composition
466 (see figure 3; supplementary data table).
467

468 **Broader constraints on determining equilibrium in melt inclusions**

469 It is commonly assumed that melt inclusion glass is in equilibrium with the host
470 mineral, based on observing whether the inclusions have euhedral 'negative crystal'
471 shapes or are rounded. The faceted negative crystal shapes are typically interpreted
472 as equilibrated, but in fact the texturally equilibrated shape moves towards rounded
473 surfaces with constant mean curvature in an attempt to minimise interfacial energy
474 (e.g. Bulau et al. 1979). Chemically, equilibrium in melt inclusions is commonly
475 tested by calculating the apparent mineral-melt K_D for the inclusion and its host
476 phenocryst, as described above for plagioclase-hosted melt inclusions. For slowly
477 equilibrating crystals, complex zoning textures in the host phase around the
478 inclusion may be clearly obvious using light microscopy or scanning electron
479 microscopy. However, in more rapidly equilibrating systems (e.g. olivine-hosted
480 inclusions) the major element Mg-Fe profiles may appear equilibrated while
481 significant chemical zoning of minor or trace components (e.g. Cr, Ni, P, Al) may still
482 be present, either within the host grain (e.g. Milman-Barris et al. 2008) or at the
483 margins of the melt inclusions (Newcombe et al. 2014). This is demonstrated by P
484 mapping of slowly cooled cumulate olivines that retained compositional zoning

485 features from a primary dendritic crystal architecture (Welsch et al. 2014).
486 Depending on whether the thermometer of choice involves major elements or trace
487 components, these issues may be significant or unimportant.
488
489 *Figure 11*
490
491 For plagioclase, diffusivities are overall much lower than in olivine, so major
492 element zonation is usually clearly evident (figure 11). Melt inclusions in plagioclase
493 commonly appear to be linked to periods of partial dissolution of the crystal,
494 suggesting that formation of a rough interface predisposes the crystals towards melt
495 entrapment. The main problem is usually to to deduce which part of the host crystal
496 most likely represents 'equilibrium' host plagioclase; in some cases this may be
497 possible from careful examination of the plagioclase zoning textures (figure 11;
498 Blundy and Cashman 2005; Humphreys et al. 2008). In other cases, petrographic
499 examination shows that melt inclusions form an irregular, interconnected network
500 in 3D, linked to either significant partial dissolution of the crystal during its
501 evolution (reaction-controlled entrapment), or skeletal or hopper growth forms
502 (growth entrapment). It may be very difficult to distinguish these two processes,
503 particularly in crystals where partial textural equilibration has occurred leading to
504 rounding of primary skeletal facets. Similar textures to those observed in plagioclase
505 are also seen in both hornblende-hosted and pyroxene-hosted melt inclusions, and
506 we suggest that further careful X-ray mapping in olivine is likely to show that these
507 same processes are also present in olivine-hosted melt inclusions.

Implications

An analysis of variations in temperature calculated using two published plagioclase-liquid thermometers shows that disequilibrium conditions can result in significant temperature overestimates for the system melt-plagioclase-H_2O. Differences in temperature calculated by the different models imply that *absolute* temperatures returned by the models should not be used with too much certainty. Systematic variations in both calculated temperature and K_D are observed with increasing decompression rate in isothermal decompression experiments. This implies that disequilibrium degassing of H_2O from the melt is an important control on calculated temperatures, and/or that growth of the equilibrium feldspar composition becomes impeded during H_2O degassing as melt viscosity and species diffusivities increase. Several natural melt inclusions datasets were examined and each shows a clear trend of apparent heating with decreasing melt H_2O content. This could imply that significant latent heating during degassing-induced crystallisation is a generic feature of subduction zone volcanoes, or that syn-eruptive or post-entrapment H_2O loss from melt inclusions during disequilibrium crystallisation is a significant process in degassing magmas. We suggest that the calculated temperatures should be treated as maxima unless there is direct evidence of equilibrium between plagioclase and melt.

Acknowledgements

MCSH acknowledges support from a Royal Society University Research Fellowship. We are grateful to Caroline Martel for provision of unpublished glass compositional data and to Becky Lange and Laura Waters for discussion and advance access to their recalibrated hygrometer. We acknowledge useful discussions with Jon Blundy, Kathy Cashman, Keith Putirka, Tom Sisson and Julia Hammer, and journal reviews from Fidel Costa and an anonymous reviewer.

References

Arculus, R.J., and Wills, K.J.A. (1980) The petrology of plutonic blocks and inclusions from the Lesser Antilles Island Arc. Journal of Petrology, 21, 743–799.

Blundy, J., and Cashman, K. (2001) Ascent-driven crystallisation of dacite magmas at Mount St Helens, 1980–1986. Contributions to Mineralogy and Petrology, 140, 631–650.

——— (2005) Rapid decompression-driven crystallization recorded by melt inclusions from Mount St. Helens volcano. Geology, 33, 793–796.

Blundy, J., Cashman, K., and Humphreys, M. (2006) Magma heating by decompression-driven crystallization beneath andesite volcanoes. Nature, 443, 76–80.

Blundy, J., Cashman, K.V., and Berlo, K. (2008) Evolving magma storage conditions beneath Mount St. Helens inferred from chemical variations in melt inclusions from the 1980-1986 and current (2004-2005) eruptions. In A volcano rekindled: The renewed eruption of Mount St. Helens, 2004-2006 Vol. 1750, pp. 755–790.

Botcharnikov, R.E., Holtz, F., Almeev, R.R., Sato, H., and Behrens, H. (2008) Storage conditions and evolution of andesitic magma prior to the 1991–95 eruption of Unzen volcano: Constraints from natural samples and phase equilibria experiments. Journal of Volcanology and Geothermal Research, 175, 168–180.

Bowen, N.L. (1913) The melting phenomena of the plagioclase feldspar. American Journal of Science, 35, 577–599.

Brugger, C.R., and Hammer, J.E. (2010) Crystallization Kinetics in Continuous Decompression Experiments: Implications for Interpreting Natural Magma Ascent Processes. Journal of Petrology, 51, 1941–1965.

Bulau, J.R., Waff, H.S., and Tyburczy, J.A. (1979) Mechanical and thermodynamic constraints on fluid distribution in partial melts. Journal of Geophysical Research, 84, 6102–6108.

Cashman, K., and Blundy, J. (2000) Degassing and crystallization of ascending andesite and dacite. Philosophical Transactions of the Royal Society of London. Series A: Mathematical, Physical and Engineering Sciences, 358, 1487–1513.

——— (2013) Petrological cannibalism: the chemical and textural consequences of incremental magma body growth. Contributions to Mineralogy and Petrology, 166, 703–729.

Cichy, S.B., Botcharnikov, R.E., Holtz, F., and Behrens, H. (2011) Vesiculation and Microlite Crystallization Induced by Decompression: a Case Study of the 1991-1995 Mt Unzen Eruption (Japan). Journal of Petrology, 52, 1469–1492.

Couch, S., Sparks, R.S.J., and Carroll, M.R. (2001) Mineral disequilibrium in lavas explained by convective self-mixing in open magma chambers. Nature, 411, 1037–1039.

Couch, S., Harford, C.L., Sparks, R.S.J., and Carroll, M.R. (2003a) Experimental constraints on the conditions of formation of highly calcic plagioclase microlites at the Soufrière Hills Volcano, Montserrat. Journal of Petrology, 44, 1455–1475.

Couch, S., Sparks, R.S.J., and Carroll, M.R. (2003b) The kinetics of degassing-induced crystallization at Soufriere Hills Volcano, Montserrat. Journal of Petrology, 44, 1477–1502.

Crabtree, S.M., and Lange, R.A. (2011) Complex Phenocryst Textures and Zoning Patterns in Andesites and Dacites: Evidence of Degassing-Induced Rapid Crystallization? Journal of Petrology, 52, 3–38.

Devine, J.D., Rutherford, M.J., Norton, G.E., and Young, S.R. (2003) Magma storage region processes inferred from geochemistry of Fe-Ti oxides in andesitic magma, Soufriere Hills Volcano, Montserrat, W.I. Journal of Petrology, 44, 1375–1400.

Drake, M.J. (1976) Plagioclase-melt equilibria. Geochimica et Cosmochimica Acta, 40, 457–465.

Dunbar, N.W., Jacobs, G.K., and Naney, M.T. (1995) Crystallization processes in an artificial magma: variations in crystal shape, growth rate and composition with melt cooling history. Contributions to Mineralogy and Petrology, 120, 412–425.

Gamble, R.P., and Taylor, L.A. (1980) Crystal/ liquid partitioning in augite: Effects of cooling rate. Earth and Planetary Science Letters, 47, 21–33.

Geschwind, C.-H., and Rutherford, M.J. (1995) Crystallization of microlites during magma ascent: the fluid mechanics of 1980–1986 eruptions at Mount St Helens. Bulletin of Volcanology, 57, 356–370.

Gualda, G.A.R., Ghiorso, M.S., Lemons, R.V., and Carley, T.L. (2012) Rhyolite-MELTS: a Modified Calibration of MELTS Optimized for Silica-rich, Fluid-bearing Magmatic Systems. Journal of Petrology, 53, 875–890.

Hamada, M., and Fujii, T. (2007) H2O-rich island arc low-K tholeiite magma inferred from Ca-rich plagioclase-melt inclusion equilibria. Geochemical Journal, 41, 437–461.

Hammer, J.E., and Rutherford, M.J. (2002) An experimental study of the kinetics of decompression-induced crystallization in silicic melt. Journal of Geophysical Research, 107.

Housh, T.B., and Luhr, J.F. (1991) Plagioclase-melt equilibria in hydrous systems. American Mineralogist, 76, 477–492.

Humphreys, M., Blundy, J., and Sparks, R. (2008) Shallow-level decompression crystallisation and deep magma supply at Shiveluch Volcano. Contributions to Mineralogy and Petrology, 155, 45–61.

Humphreys, M., Edmonds, M., Christopher, T., and Hards, V. (2009a) Chlorine variations in the magma of Soufriere Hills Volcano, Montserrat: Insights from Cl in hornblende and melt inclusions. Geochimica et Cosmochimica Acta, 73, 5693–5708.

Humphreys, M., Christopher, T., and Hards, V. (2009b) Microlite transfer by disaggregation of mafic inclusions following magma mixing at Soufriere Hills volcano, Montserrat. Contributions to Mineralogy and Petrology, 157, 609–624.

Humphreys, M., Edmonds, M., Christopher, T., and Hards, V. (2010) Magma hybridisation and diffusive exchange recorded in heterogeneous glasses from Soufriere Hills Volcano, Montserrat. Geophysical Research Letters, 37.

Johannes, W. (1984) Beginning of melting in the granite system Qz-Or-Ab-An-H2O. Contributions to Mineralogy and Petrology, 86, 264–273.

Kennedy, A.., Lofgren, G.E., and Wasserburg, G.J. (1993) An experimental study of trace element partitioning between olivine, orthopyroxene and melt in chondrules: equilibrium values and kinetic effects. Earth and Planetary Science Letters, 115, 177–195.

Kudo, A.M., and Weill, D.F. (1970) An igneous plagioclase thermometer. Contributions to Mineralogy and Petrology, 25, 52–65.

629 Lange, R.A., Frey, H.M., and Hector, J. (2009) A thermodynamic model for the
630 plagioclase-liquid hygrometer/thermometer. American Mineralogist, 94, 494–506.

631 Mann, C.P., Wallace, P.J., and Stix, J. (2013) Phenocryst-hosted melt inclusions record
632 stalling of magma during ascent in the conduit and upper magma reservoir prior to
633 vulcanian explosions, Soufriere Hills volcano, Montserrat, West Indies. Bulletin
634 of Volcanology, 75, 687.

635 Martel, C., and Schmidt, B.C. (2003) Decompression experiments as an insight into
636 ascent rates of silicic magmas. Contributions to Mineralogy and Petrology, 144,
637 397–415.

638 Milman-Barris, M.S., Beckett, J.R., Baker, M.B., Hofmann, A.E., Morgan, Z., Crowley,
639 M.R., Vielzeuf, D., and Stolper, E. (2008) Zoning of phosphorus in igneous
640 olivine. Contributions to Mineralogy and Petrology, 155, 739–765.

641 Mollo, S., Del Gaudio, P., Ventura, G., Iezzi, G., and Scarlato, P. (2010) Dependence of
642 clinopyroxene composition on cooling rate in basaltic magmas: Implications for
643 thermobarometry. Lithos, 118, 302–312.

644 Mollo, S., Putirka, K., Iezzi, G., Del Gaudio, P., and Scarlato, P. (2011) Plagioclase–melt
645 (dis)equilibrium due to cooling dynamics: Implications for thermometry,
646 barometry and hygrometry. Lithos, 125, 221–235.

647 Newcombe, M.E., Fabbrizio, A., Zhang, Y., Ma, C., Voyer, M.L., Guan, Y., Eiler, J.M.,
648 Saal, A.E., and Stolper, E.M. (2014) Chemical zonation in olivine-hosted melt
649 inclusions. Contributions to Mineralogy and Petrology, 168, 1–26.

650 Newman, S., and Lowenstern, J.B. (2002) VolatileCalc: a silicate melt–H2O-CO2
651 solution model written in Visual Basic for excel. Computers & Geosciences, 28,
652 597–604.

653 Panjasawatwong, Y., Danyushevsky, L.V., Crawford, A.J., and Harris, K.L. (1995) An
654 experimental study of the effects of melt composition on plagioclase-melt
655 equilibria at 5 and 10 kbar: implications for the origin of magmatic high-An
656 plagioclase. Contributions to Mineralogy and Petrology, 118, 420–432.

657 Pichavant, M., Costa, F., Burgisser, A., Scaillet, B., Martel, C., and Poussineau, S. (2007)
658 Equilibration Scales in Silicic to Intermediate Magmas Implications for
659 Experimental Studies. Journal of Petrology, 48, 1955–1972.

660 Putirka, K., and Condit, C.D. (2003) Cross section of a magma conduit system at the
661 margin of the Colorado Plateau. Geology, 31, 701–704.

662 Putirka, K.D. (2005) Igneous thermometers and barometers based on plagioclase + liquid
663 equilibria: Tests of some existing models and new calibrations. American
664 Mineralogist, 90, 336–346.

——— (2008) Thermometers and barometers for volcanic systems. In Minerals, Inclusions, and Volcanic Processes Vol. 69, pp. 61–120.

Ridolfi, F., Renzulli, A., and Puerini, M. (2010) Stability and chemical equilibrium of amphibole in calc-alkaline magmas: an overview, new thermobarometric formulations and application to subduction-related volcanoes. Contributions to Mineralogy and Petrology, 160, 45–66.

Rutherford, M.J., and Devine, J.D. (2003) Magmatic conditions and magma ascent as indicated by hornblende phase equilibria and reactions in the 1995-2002 Soufriere Hills magma. Journal of Petrology, 44, 1433–1454.

Sisson, T.W., and Grove, T.L. (1993) Experimental investigations of the role of H2O in calc-alkaline differentiation and subduction zone magmatism. Contributions to Mineralogy and Petrology, 113, 143–166.

Waters, L.E. (2013) The effect of degassing of H2O on crystallization and oxidation in highly evolved magmas: Implications for the origin of rhyolite liquids. PhD, University of Michigan.

Waters, L.E., and Lange, R.A. (n.d.) An updated calibration of the plagioclase-liquid hygrometer-thermometer applicable to basalts through rhyolites. American Mineralogist (in press).

Welsch, B., Hammer, J., and Hellebrand, E. (2014) Phosphorus zoning reveals dendritic architecture of olivine. Geology, 42, 867–870.

687 Figure 1

688 Equilibrium relationships between rhyolitic melt H_2O,temperature and plagioclase
689 XAn, calculated using Putirka (2005) and Lange et al. (2009). (a) Contours of
690 constant plagioclase composition in H_2O-T space. Large grey diamonds are
691 interpolated from the phase diagram of Couch et al. (2003). (b) Contours of constant
692 temperature in H_2O-X_{An} space. Also shown is RhyoliteMELTS modelling of
693 isothermal decompression for rhyolitic melt (bold lines, 825-875 °C) and basaltic
694 andesite melt (thin black lines, 1000-1100 °C).

695

696 Figure 2

697 Contours of constant pressure (assuming H_2O saturation, i.e. P_{tot} = pH_2O) in T–X_{An}
698 space, calculated for rhyolitic melt using Putirka (2005) and Lange et al. (2009).
699 Large circles are interpolated from the phase diagram of Couch et al. (2003) for 160
700 MPa (black) and 200 MPa (grey). Also shown is RhyoliteMELTS modelling of
701 isobaric cooling in rhyolitic melt (25-200 MPa).

702

703 Figure 3

704 Theoretical variation of plagioclase-liquid K_D for rhyolitic melt (as defined by
705 Putirka 2005; 2008) with calculated temperature (T_{calc}) as a function of pressure
706 (assuming H_2O saturation, i.e. P_{tot} = pH_2O) (a), and with pH_2O as a function of
707 temperature (b). Points in (a) represent increments of 10 mol% X_{An}.

708

709 Figure 4

H_2O concentration in experimentally decompressed glasses from Martel & Schmidt (2003), Brugger & Hammer (2010) and Cichy et al. (2011), in comparison with isobaric (solubility) data from Mangan & Sisson (2000). Also shown is rhyolite solubility curve from VolatileCalc (Newman & Lowenstern 2002). All data have H_2O concentrations in excess of the solubility limit for the experimental quench pressure, indicating kinetically inhibited degassing.

Figure 5

Variation of calculated temperature (T_{calc}, using model A from Putirka, 2005) and K_D with pH_2O in experimentally decompressed glasses from Brugger & Hammer (2010; a, b), Cichy et al. (2011; c, d) and Martel & Schmidt (2003; e, f). Grey bar with black line shows the experimental run temperature in each case ± 5 °C. See supplementary data table for original data and calculated values.

Figure 6

Variation of calculated temperature (T_{calc}, using model A from Putirka, 2005) and K_D with decompression rate in experimentally decompressed glasses from Brugger & Hammer (2010; a, b), Cichy et al. (2011; c, d) and Martel & Schmidt (2003; e, f). Grey bar with black line shows the experimental run temperature in each case ± 5 °C. See supplementary data table for original data and calculated values.

Figure 7

(a) Variation of calculated temperature (T_{calc}, using model A from Putirka, 2005) with H_2O concentration reported for plagioclase-hosted melt inclusions from Soufrière Hills, Montserrat (Humphreys et al. 2009); Mt Unzen, Japan (Botcharnikov et al. 2007); Mount St Helens, USA (Blundy et al. 2006); Shiveluch, Kamchatka (Blundy et al. 2006) and Izu Oshima (Hamada & Fujii 2007). Constant-X_{An} contours are shown for comparison (symbols as figure 1). (b) Variations of calculated temperature with reported X_{An} of the host plagioclase phenocryst for the same melt inclusion suites. Constant-pH_2O contours are shown for comparison (symbols as figure 2). See supplementary data table for original data and calculated values.

Figure 8

Variation of calculated K_D with (a) plagioclase X_{An} and (b) glass H_2O concentration reported for melt inclusion datasets from the literature. Dark circles – Mount St Helens (Blundy et al. 2006); grey squares – Shiveluch (Blundy et al. 2006); dashes – Soufrière Hills, Montserrat (Humphreys et al. 2009); crosses - Izu Oshima (Hamada & Fujii 2007); dark triangles - Mt Unzen (Botcharnikov et al. 2007). See supplementary data table for original data and calculated values.

Figure 9

Regression of calculated temperature with each of the parameters that make up the 'model A' calculation (Putirka 2005), (a) Ca_L, (b) Na_L, (c) Al_L, (d) Si_L, (e) H_2O and (f) X_{An}. Dark circles – Mount St Helens, grey squares – Shiveluch (Blundy et al. 2006). Linear regression trends and equations are given for any significant regressions (R^2

755 ≥ 0.15), with Mount St Helens regressions in black and Shiveluch in grey. The most
756 significant parameter controlling T_{calc} is the H_2O content of the glass. See
757 supplementary data table for original data and calculated values.
758
759 Figure 10
760 Regression of calculated temperature with each of the parameters that make up the
761 'model A' calculation (Putirka 2005), (a) Ca_L, (b) Na_L, (c) Al_L, (d) Si_L, (e) H_2O and (f)
762 X_{An}. Dashes – Soufriere Hills, Montserrat (Humphreys et al. 2009); crosses - Izu
763 Oshima (Hamada & Fujii 2007); dark triangles - Mt Unzen (Botcharnikov et al.
764 2008). Linear regression trends and equations are given for any significant
765 regressions (R^2 ≥ 0.15) in each dataset. The most significant parameter controlling
766 T_{calc} is the H_2O content of the glass. See supplementary data table for original data
767 and calculated values.
768
769 Figure 11
770 Back-scattered SEM image illustrating the complexity of plagioclase zoning that is
771 common in intermediate calc-alkaline lavas. Melt inclusions are dark blebs (some
772 annotated 'MI'). White dashed lines outline clear resorptive zoning 'events' that
773 leave irregular boundaries and may entrap melt inclusions.
774

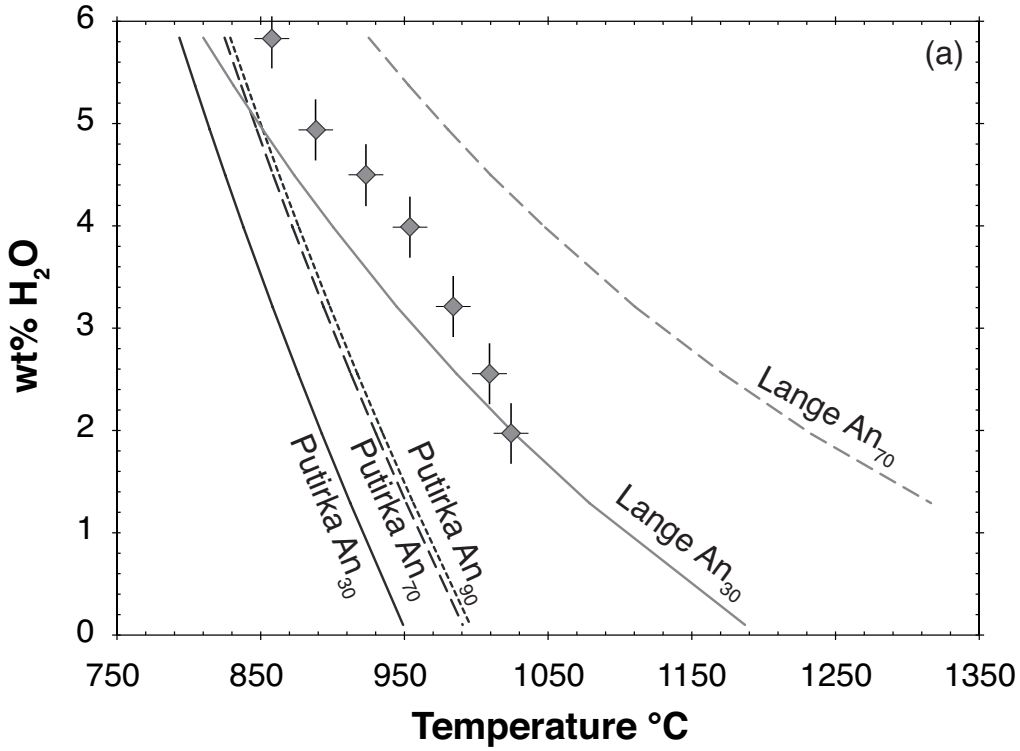
(a)
wt% H2O
Temperature °C
Lange An70
Lange An30
Putirka An90
Putirka An70
Putirka An30

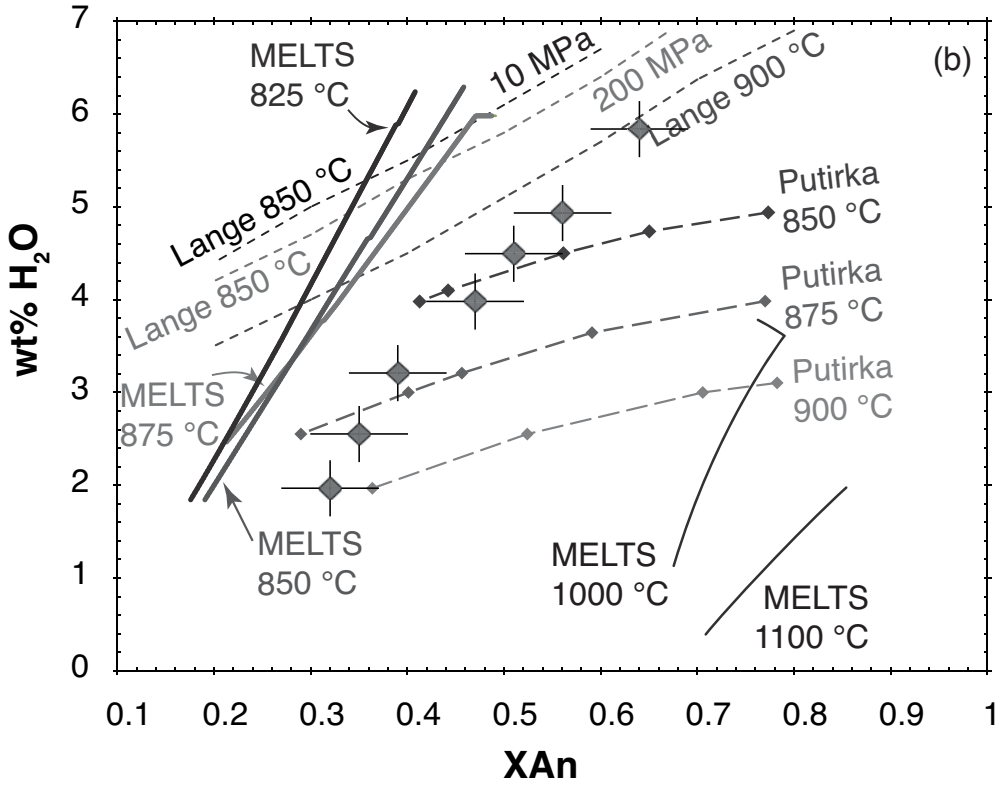
(b)
wt% H2O
XAn
MELTS 825 °C
10 MPa
200 MPa
Lange 900 °C
Lange 850 °C
Lange 850 °C
Putirka 850 °C
Putirka 875 °C
Putirka 900 °C
MELTS 875 °C
MELTS 850 °C
MELTS 1000 °C
MELTS 1100 °C

Figure 1

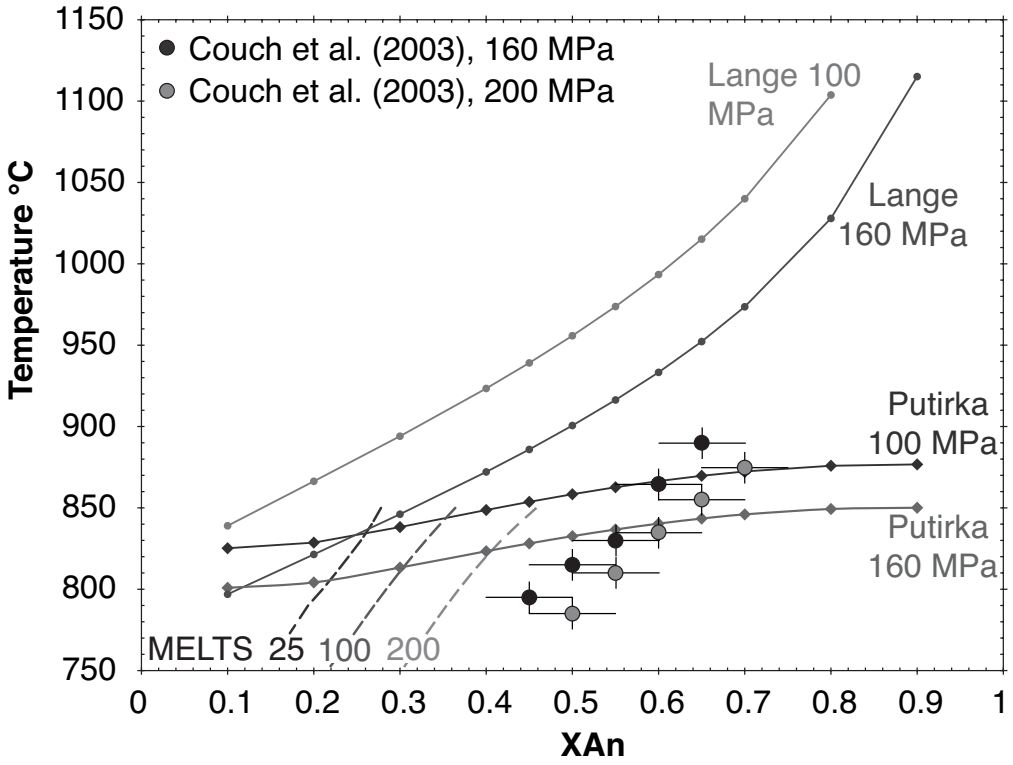
Couch et al. (2003), 160 MPa
Couch et al. (2003), 200 MPa
Lange 100 MPa
Lange 160 MPa
Putirka 100 MPa
Putirka 160 MPa
MELTS 25 100 200
Temperature °C
XAn
1150
1100
1050
1000
950
900
850
800
750
0
0.1
0.2
0.3
0.4
0.5
0.6
0.7
0.8
0.9
1

Figure 2

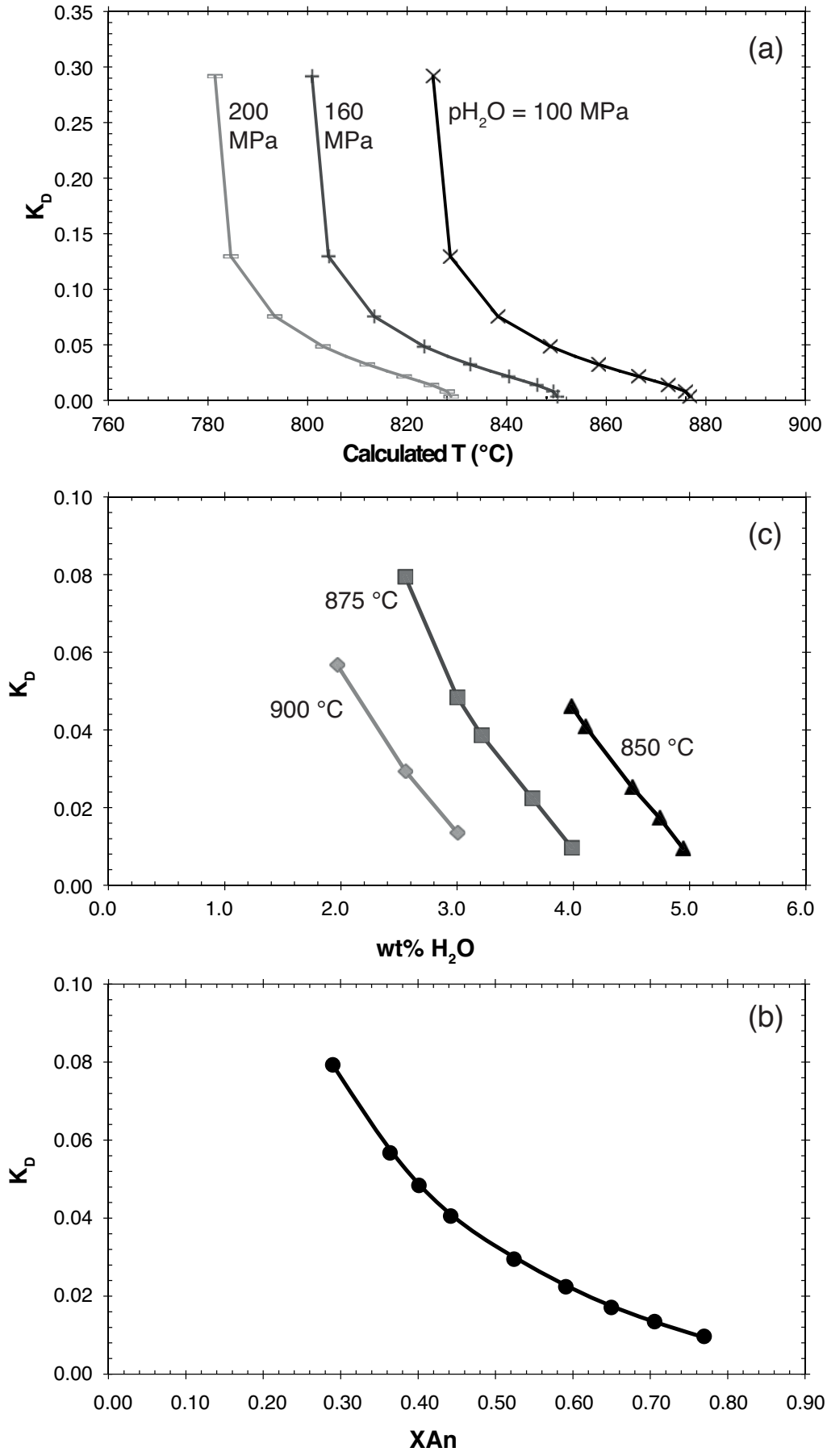
(a)
200 MPa
160 MPa
pH2O = 100 MPa
KD
Calculated T (°C)
(c)
875 °C
900 °C
850 °C
KD
wt% H2O
(b)
KD
XAn

Figure 3

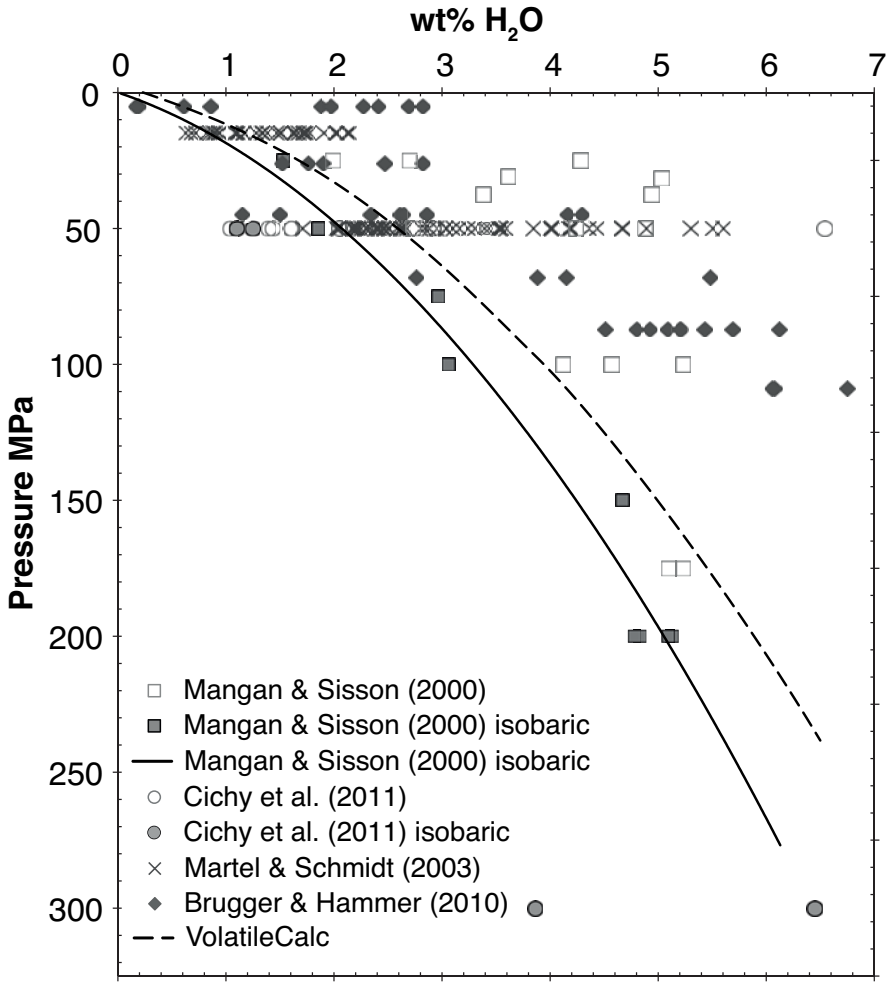
wt% H2O
0
1
2
3
4
5
6
7
Pressure MPa
0
50
100
150
200
250
300
Mangan & Sisson (2000)
Mangan & Sisson (2000) isobaric
Mangan & Sisson (2000) isobaric
Cichy et al. (2011)
Cichy et al. (2011) isobaric
Martel & Schmidt (2003)
Brugger & Hammer (2010)
VolatileCalc

Figure 4

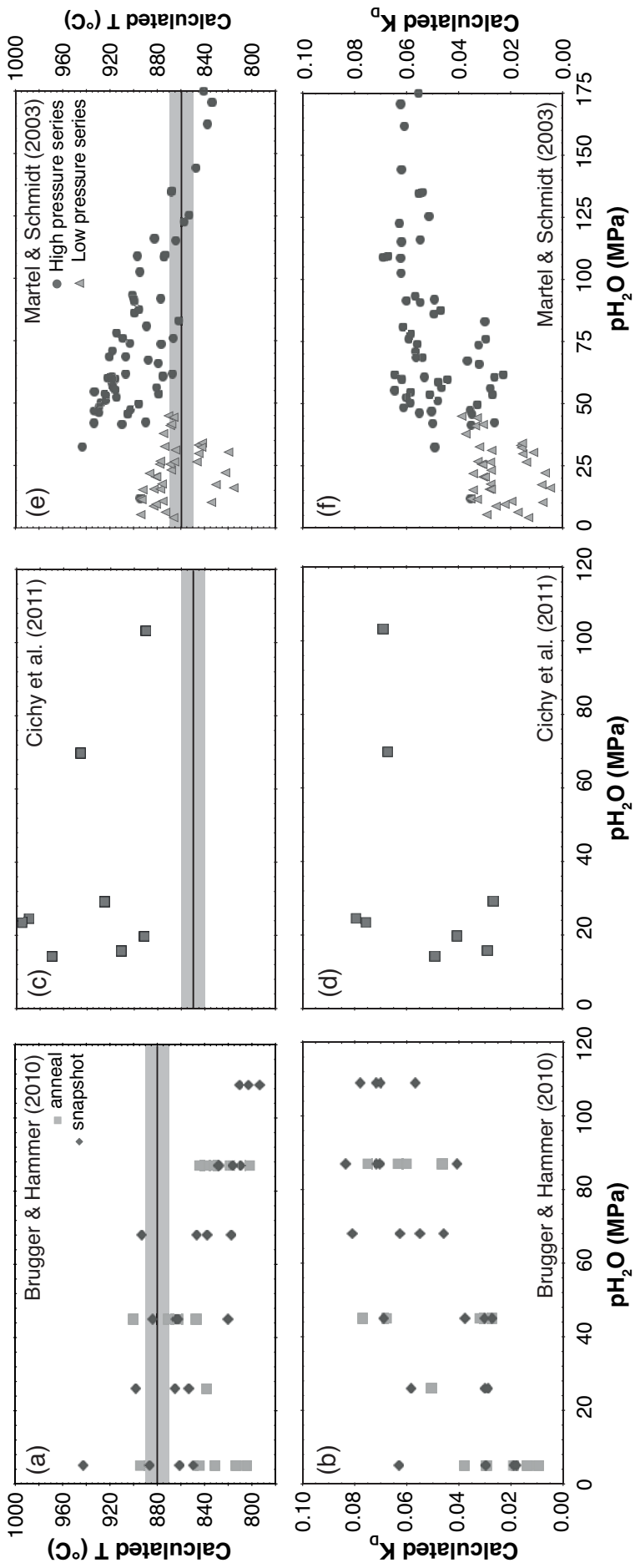
(a)
Brugger & Hammer (2010)
anneal
snapshot
Calculated T (°C)
1000
960
920
880
840
800
(b)
Brugger & Hammer (2010)
Calculated K_D
0.10
0.08
0.06
0.04
0.02
0.00
pH_2O (MPa)
0
20
40
60
80
100
120
(c)
Cichy et al. (2011)
(d)
Cichy et al. (2011)
(e)
Martel & Schmidt (2003)
High pressure series
Low pressure series
(f)
Martel & Schmidt (2003)
pH_2O (MPa)
0
25
50
75
100
125
150
175

Figure 5

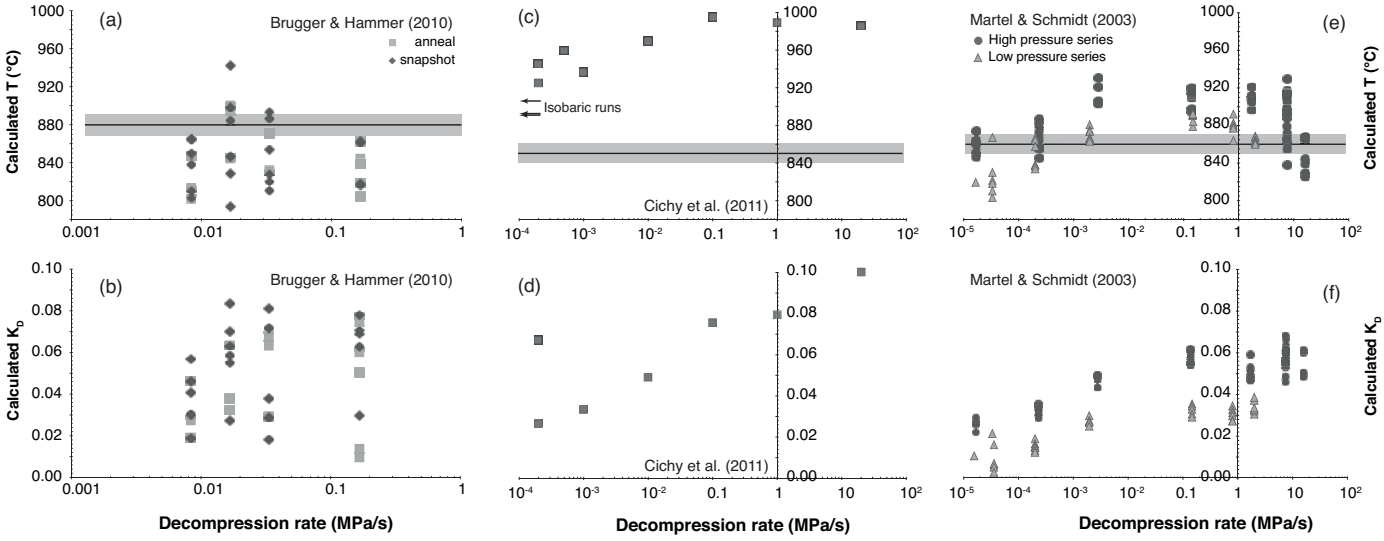
(a)
Brugger & Hammer (2010)
anneal
snapshot
Calculated T (°C)
(b)
Brugger & Hammer (2010)
Calculated K_D
Decompression rate (MPa/s)
(c)
Isobaric runs
Cichy et al. (2011)
(d)
Cichy et al. (2011)
Decompression rate (MPa/s)
Martel & Schmidt (2003)
High pressure series
Low pressure series
(e)
Calculated T (°C)
Martel & Schmidt (2003)
(f)
Calculated K_D
Decompression rate (MPa/s)

Figure 6

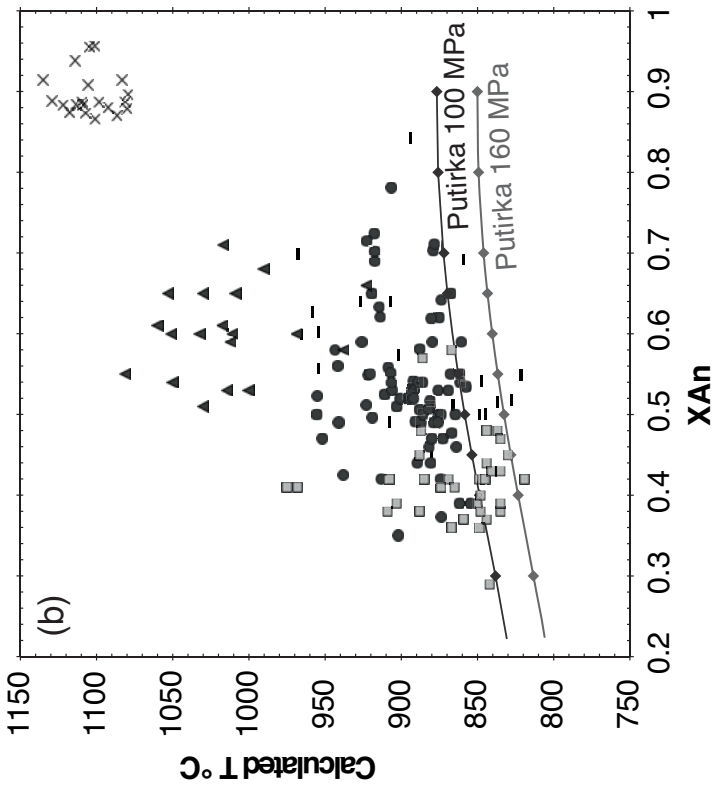
(b)
Putirka 100 MPa
Putirka 160 MPa
Calculated T °C
XAn
1150
1100
1050
1000
950
900
850
800
750
0.2
0.3
0.4
0.5
0.6
0.7
0.8
0.9
1

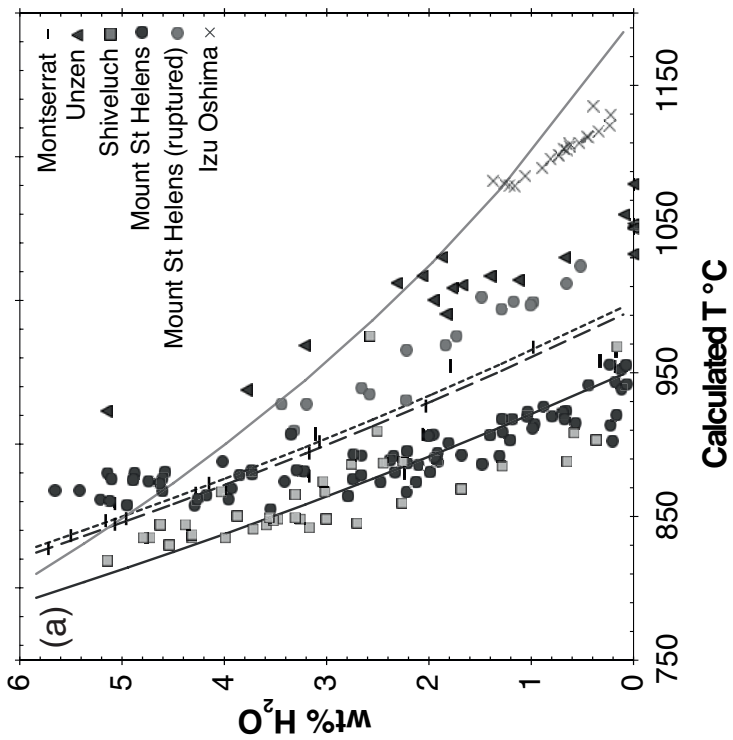
(a)
Montserrat
Unzen
Shiveluch
Mount St Helens
Mount St Helens (ruptured)
Izu Oshima
wt% H2O
Calculated T °C
6
5
4
3
2
1
0
750
850
950
1050
1150

Figure 7

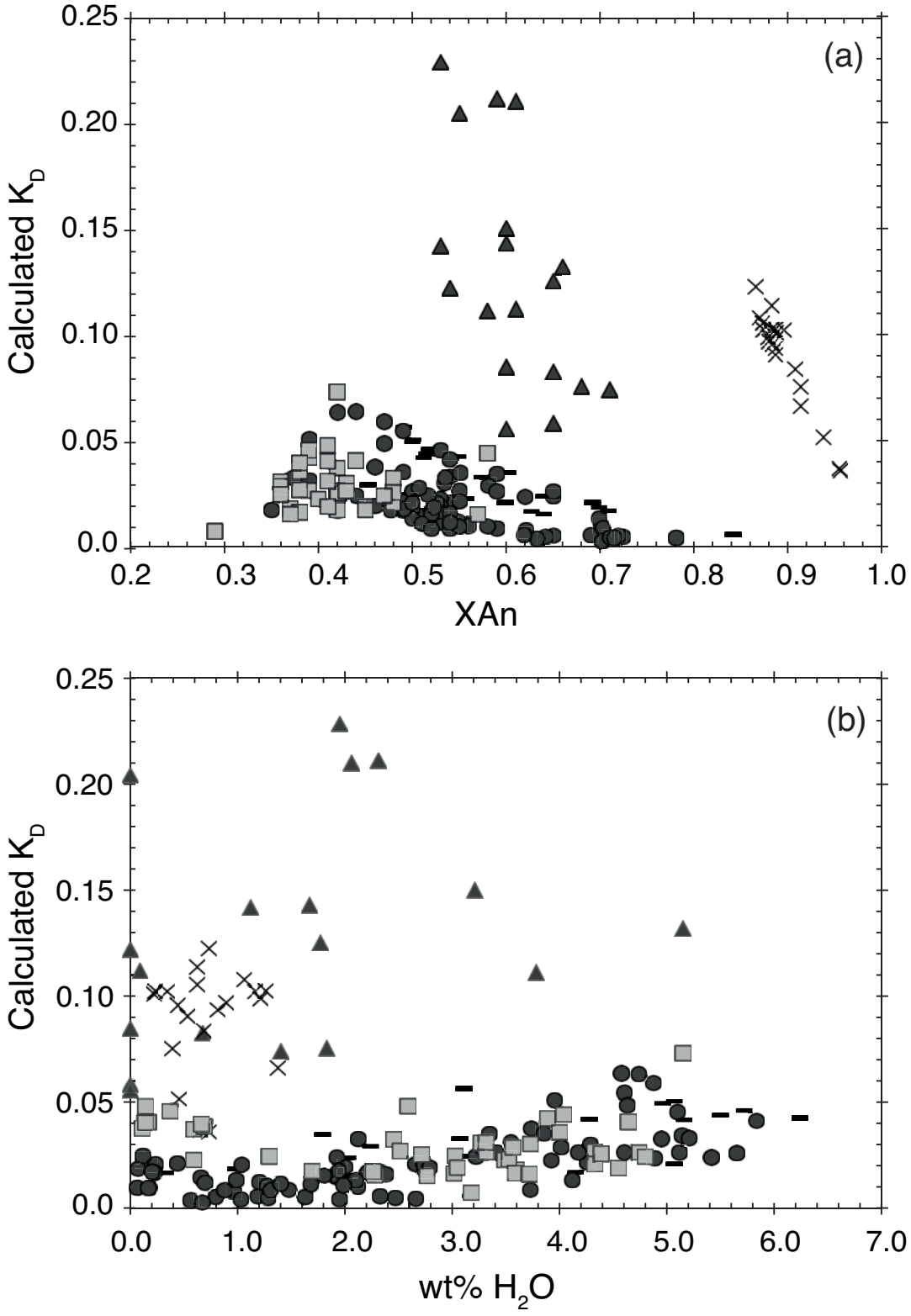
(a)
Calculated K_D
XAn
0.25
0.20
0.15
0.10
0.05
0.0
0.2
0.3
0.4
0.5
0.6
0.7
0.8
0.9
1.0
(b)
Calculated K_D
wt% H_2O
0.0
1.0
2.0
3.0
4.0
5.0
6.0
7.0

Figure 8

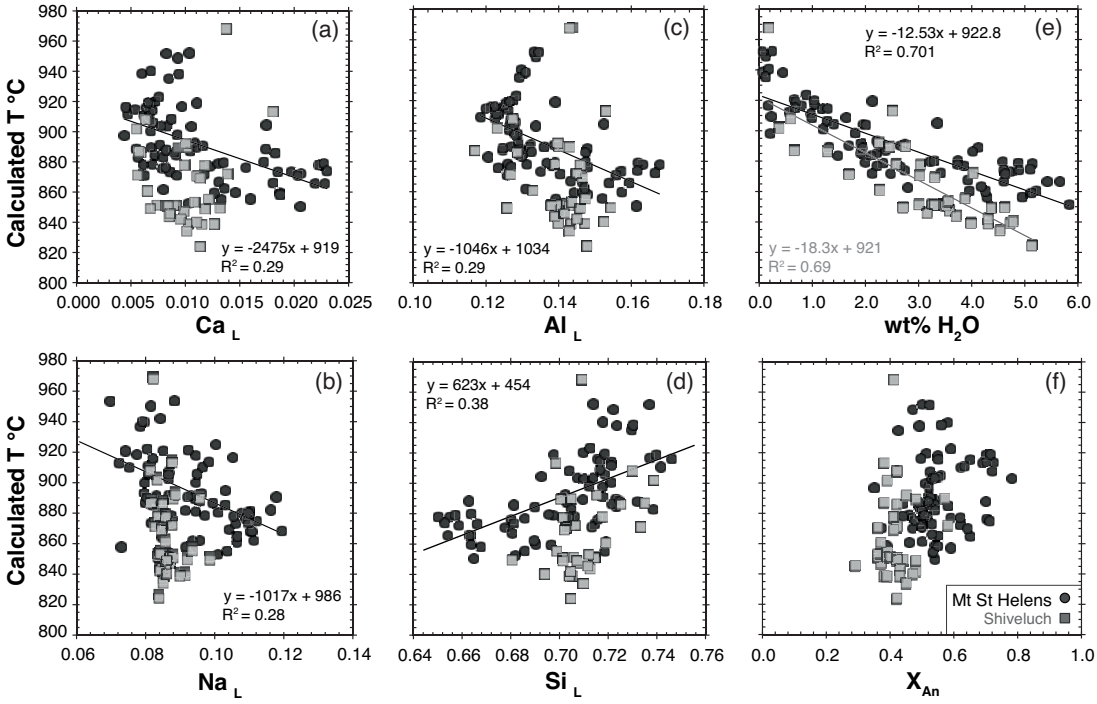
Calculated T °C
(a)
y = -2475x + 919
R² = 0.29
Ca L
(c)
y = -1046x + 1034
R² = 0.29
Al L
(e)
y = -12.53x + 922.8
R² = 0.701
y = -18.3x + 921
R² = 0.69
wt% H2O
(b)
y = -1017x + 986
R² = 0.28
Na L
(d)
y = 623x + 454
R² = 0.38
Si L
(f)
Mt St Helens
Shiveluch
XAn

Figure 9

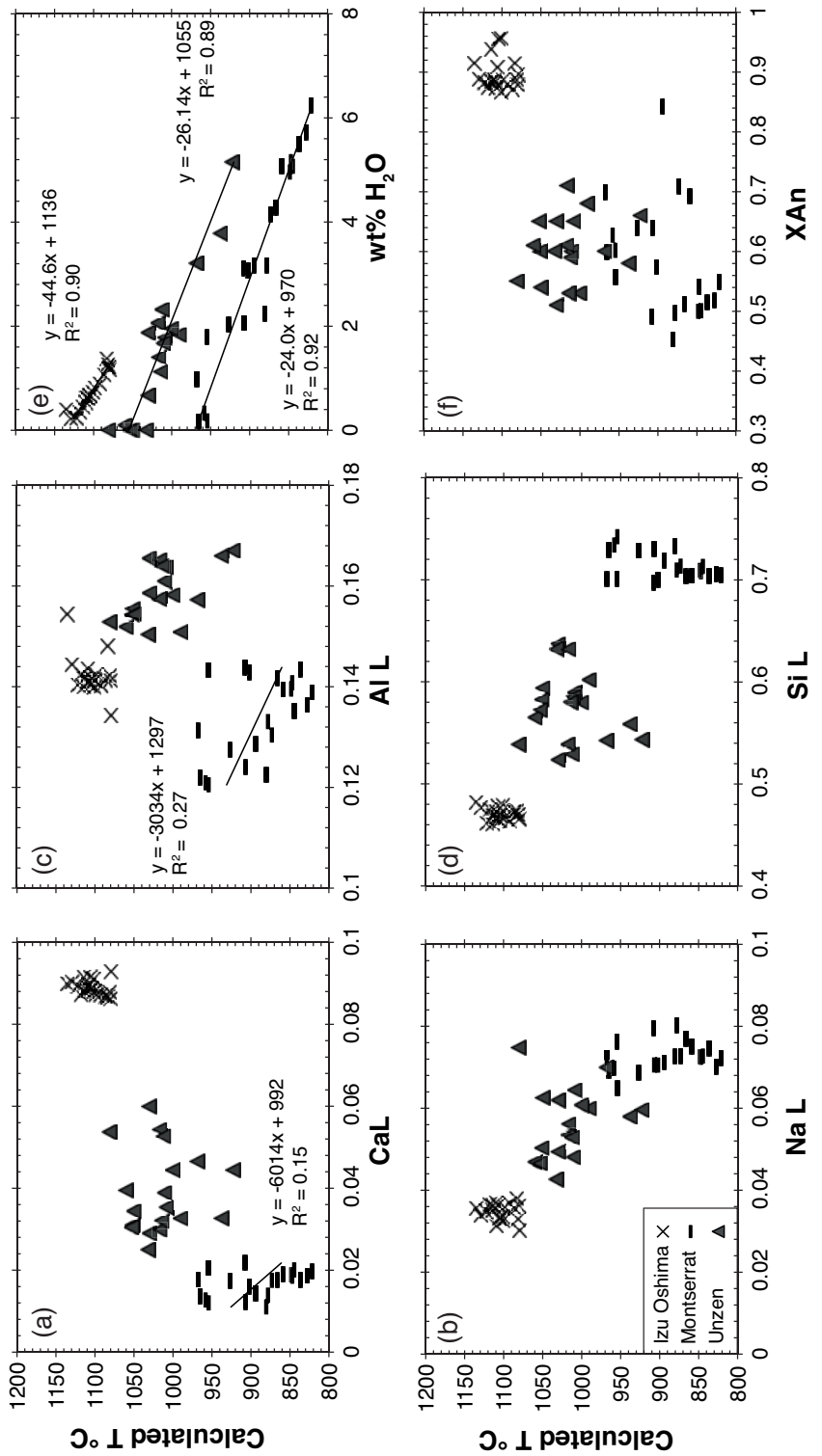
(a)
y = -6014x + 992
R² = 0.15
CaL
Calculated T °C
(b)
Izu Oshima ×
Montserrat
Unzen
Na L
(c)
y = -3034x + 1297
R² = 0.27
Al L
(d)
Si L
(e)
y = -44.6x + 1136
R² = 0.90
y = -26.14x + 1055
R² = 0.89
y = -24.0x + 970
R² = 0.92
wt% H2O
(f)
XAn

Figure 10

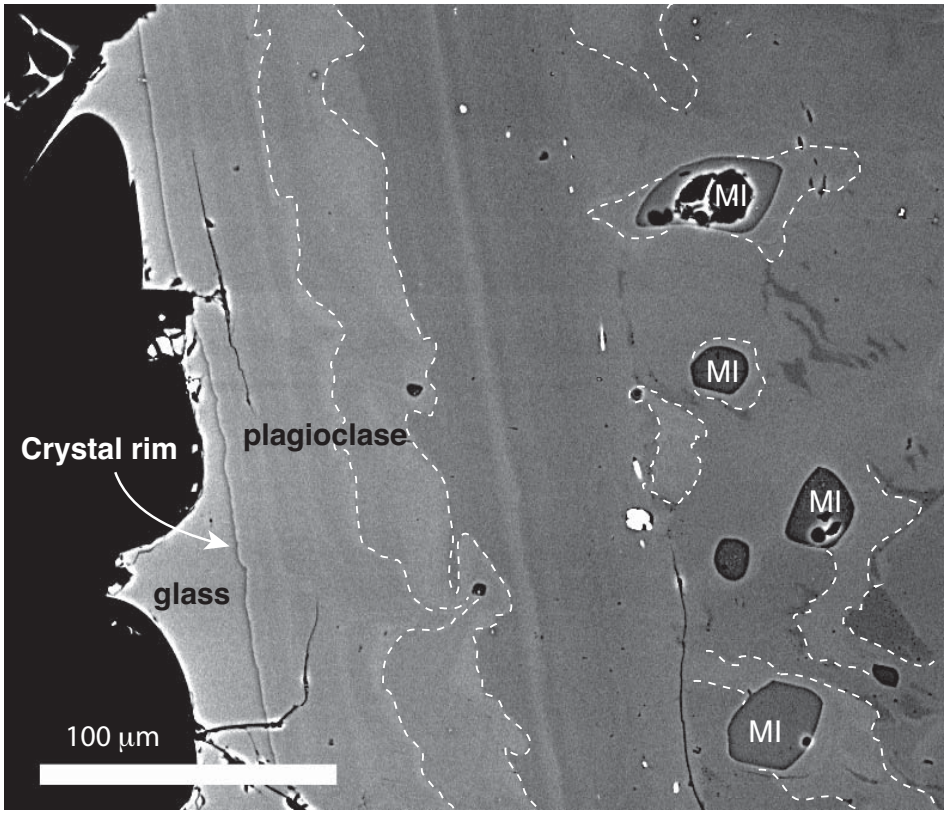

Figure 11

	MVO1524b_112	ol101mi1
SiO_2	73.32	52.20
TiO_2	0.26	0.86
Al_2O_3	11.66	15.80
FeO_T	1.56	12.40
MgO	0.28	5.72
MnO	0.07	0.22
CaO	1.34	10.34
Na_2O	4.28	1.82
K_2O	2.54	0.31
Cl	0.26	0.04
H_2O	3.16	1.24
Total	98.73	100.95

Table 1.
Composition of rhyolite melt inclusion (MVO1524b_112, from Humphreys et al. 2009) and basaltic andesite melt (ol101mi1, from Hamada & Fujii 2007) used for MELTS modelling and calculations shown in figures 1-4.